IEEE Open Journal of
Power Electronics

Received 15 May 2024; accepted 12 June 2024. Date of publication 20 June 2024;
date of current version 27 June 2024. The review of this article was arranged by Associate Editor Chandan Kumar.

Digital Object Identifier 10.1109/OJPEL.2024.3416339

Ancillary Service Provision via Primal-Dual Based Coordination of Distributed Power Electronic Converters in Three-Phase Microgrids

ANDREA LAURI [1] (Graduate Student Member, IEEE), TOMMASO CALDOGNETTO [1] (Senior Member, IEEE), RUGGERO CARLI [2] (Member, IEEE), DAVIDE BIADENE [1] (Member, IEEE), AND PAOLO MATTAVELLI [1] (Fellow, IEEE)

[1]Department of Management and Engineering, 36100 Vicenza, Italy
[2]Department of Information Engineering, 35131 Padova, Italy

CORRESPONDING AUTHORS: ANDREA LAURI; TOMMASO CALDOGNETTO (e-mail: andrea.lauri@phd.unipd.it; tommaso.caldognetto@unipd.it).

This work was supported in part by the National Recovery and Resilience Plan (NRRP), Mission 4 Component 2 Investment 1.3 - Call for tender no. 0341 published on 15.03.2022 by the Italian Ministry of University and Research (MUR), in part by the European Union–NextGenerationEU-Project Title "Network 4 Energy Sustainable Transition – NEST", project code PE0000021, Concession Decree No. 1561 of 11.10.2022 by MUR CUP C93C22005230007, in part by the National Recovery and Resilience Plan (NRRP), Mission 4, Component 2, Investment 1.1, Call for tender no. 1409 published on 14.09.2022 by the Italian Ministry of University and Research (MUR), and in part by the European Union–NextGenerationEU–Project Title RESCOPE4GREEN(P2022W4HFX)-CUP C53D23007290001-Grant Assignment Decree No. 1383 adopted on 01.09.2023 by the Italian Ministry of University and Research (MUR).

ABSTRACT Electronic power converters are extensively applied in microgrids to interface distributed energy resources to the grid. Besides the primary active-power control, electronic converters support increasingly advanced and flexible control capabilities. While the former is typically bound to local needs (e.g., maximum power extraction from renewables), additional degrees of freedom can be exploited to support microgrid operation. This article proposes a control algorithm that allows the optimal provision of reactive power, negative-sequence, and zero-sequence currents by distributed converters. The resulting operation shows enhanced power quality at the point of common coupling (PCC) and limited conversion losses, which are taken into account in the optimization algorithm. Three modes of operation are discussed, that is, *i*) power loss minimization; *ii*) balanced currents at the PCC; *iii*) zero reactive power flow at the PCC. An algorithm based on the primal-dual method is proposed to solve the optimization problem. Results based on experimental measurements are discussed to prove the effectiveness of the proposal.

INDEX TERMS Ancillary services, microgrid, optimal operation, unbalanced distribution network.

I. INTRODUCTION

THE wide selection of control techniques for electronic power converters (EPCs) creates new degrees of freedom in the management of electrical quantities. The ability to perform unbalance regulation in three-phase EPCs, which is easily supported by grid-following converters, has also been demonstrated in grid-forming converters [1], [2], [3], [4], [5]. The goal of this research is to explore the optimal exploitation of the control flexibility of EPCs in pursuing valuable services for the upstream grid, such as, power loss reduction and unbalance compensation at the point of common coupling (PCC) with the main grid. This should be done without altering the active power flow, typically driven by other economic-related or energy-related requirements [6], [7], [8], [9], [10], [11], [12], [13], [14].

Several approaches in the literature aim at optimizing the operation of EPCs in microgrids. Some focus on microgrids connected to upstream grids, which typically prioritize energy management aspects and target transactive operations (e.g., optimal bidding or energy scheduling) [6], [7], [8], [9], [10], [11], or ancillary services markets such as frequency/voltage regulation [7], [8], [9], [10], [12], [13], [14]. However, since energy exchange is not directly related to unbalanced and reactive power, dedicated optimization strategies are required.

The method proposed in [15] mitigates the voltage unbalance by minimizing the sum of squared negative-sequence components. Still, the objective should also consider the impact on the distributed EPCs to optimize the compensation effort. A model-free consensus-based power control algorithm is proposed in [16], where a power-sharing proportional to the generators capabilities is achieved, focusing on the compensation of current unbalance at the PCC. A multiobjective optimization approach is proposed in [17], which includes stochastic aspects. The approach targets benefits in costs, reliability, and impact on the environment; the voltage unbalance is constrained inside tolerance bands. In [18], two different control levels realize voltage unbalance compensation. A bus is selected as critical, and its compensation is achieved by the lowest control level, equally sharing the compensation effort among units. Then the higher level corrects unbalance factors at other buses, bringing their value within tolerance bands; the method considers islanded operation.

None of the aforementioned methods considers that changing the operating point of distributed EPCs affects the efficiency of the generation units and, consequently, the overall system losses. Converter losses are usually modeled as quadratic functions, and Lagrange-multipliers based methods are commonly employed when solving such problems [19]. In [20], the optimal sharing of current among distributed converters is computed by solving in closed-form the Lagrange-multipliers problem. The approach is limited to the provision of active and reactive power in grid-tied operation. In [21], the Lagrange-multipliers problem is formulated to compute the droop coefficients that optimally share the reactive power in single-phase islanded microgrids. The problem is then solved iteratively using the dual-ascent algorithm.

The solution proposed in this work is based on the preliminary results presented in [22]. Herein, an improved solution method is described and verified considering a realistic application example. The proposed methodology is applied in the outlined scenario contributing in:

1) proposing a primal-dual coordination algorithm for the optimal coordination of distributed power converters in three-phase microgrids;
2) formulating the control problem to provide services like reactive and unbalanced currents while minimizing power losses and avoiding constraining the active power flows;
3) demonstrating the operation of the algorithm considering a cost function including the converters' power losses with respect to the operating point.

The method proposed herein minimizes the overall power losses, allowing to choose whether or not to constrain the PCC current flow to be perfectly balanced, with no reactive power flow. Remarkably, different convex cost functions can be considered, allowing the employment of the presented method in a vast class of problems.

In the following, Section II describes the considered scenario and control problem, which is solved by the optimization method presented in Section III. Section IV describes the experimental setup used to derive a cost function representing converters' power losses, herein considered to demonstrate the proposal. Section V illustrates the specific implementation of the proposed primal-dual based coordination method. The method is verified in Section VI, which also describes the simulation tests and benchmark used for validation. Section VII concludes the paper.

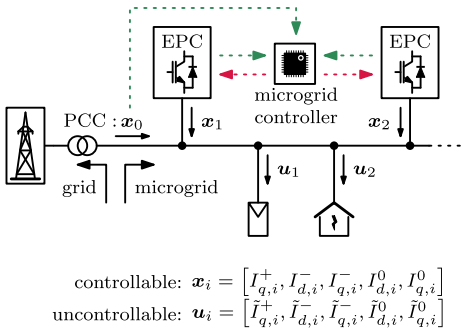

FIGURE 1. Typical application scenario for the proposed approach. Dashed paths represent communication links.

II. PROBLEM DESCRIPTION

A. ASSUMPTIONS

Fig. 1 shows a typical application scenario for the method proposed in this manuscript. The microgrid is composed of N_x controllable units $\boldsymbol{x}_i$ and N_u uncontrollable units $\boldsymbol{u}_i$. The following assumptions are made:

1) a central microgrid controller (MC) is present, capable of exchanging information with the controllable units $\boldsymbol{x}_i$, $i = 1, \ldots, N_x$, by low-bandwidth communication;
2) controllable units exploit the communication link to send to the MC data about their cost function and operating point;
3) periodically, the MC runs an optimization algorithm, and then dispatches optimal reference values to the controllable units;
4) phasors representing the voltages at the nodes of the grid have approximately equal phases along the distribution lines.

By assumption 4), it is possible to consider active power equivalent to positive-sequence d-axis current (i.e., active current), as done in other works, like [23], [24]. This is also valid for reactive power and q-axis current (i.e., reactive current), recalling that the reactive power is proportional to $-I^+_q$, according to common definitions of reactive power with d-axis aligned to grid voltage phasor and q-axis leading it by 90°. It is worth noting that the method pursued herein deals with quantities at the fundamental frequency, for which quantities like reactive power and unbalance are defined.

Let $\boldsymbol{x} \triangleq [\boldsymbol{x}_0, \ldots, \boldsymbol{x}_i, \ldots, \boldsymbol{x}_{N_x}]^\top \in \mathbb{R}^{(N_x+1)\times 1}$ be the column vector of all the optimization variables, with $\boldsymbol{x}_i = [I^+_{q,i}, I^-_{d,i}, I^-_{q,i}, I^0_{d,i}, I^0_{q,i}] \in \mathbb{R}^{1\times 5}$, namely, the rms value of the positive sequence reactive current, of the negative sequence d and q currents, the zero sequence d and q currents. Vector $\boldsymbol{x}_0$ collects the same quantities measured

at the point of common coupling (PCC). Notice that the PCC can be regarded, as commonly done, as a slack bus that provides the mismatch between absorbed and injected currents. Consequently, its contribution can be indirectly controlled by choosing the operating points $\boldsymbol{x}_i$, $i = 1, \ldots, N_x$, since (4) holds. For this reason, the PCC is included among the controllable units. The vectors containing quantities referring to uncontrollable units are defined as $\boldsymbol{u}_i \triangleq [\tilde{I}^+_{q,i}, \tilde{I}^-_{d,i}, \tilde{I}^-_{q,i}, \tilde{I}^0_{d,i}, \tilde{I}^0_{q,i}] \in \mathbb{R}^{1\times 5}$, where $\tilde{\cdot}$ denotes a non-controllable quantity.

B. COST FUNCTION

The goal of the method is to optimally provide controllable quantities, minimizing herein a cost function representing power losses. Other cost functions may be considered for the implementation of the approach.

The considered cost function accounts for converter losses and the power losses at the PCC interface as:

$$F(\boldsymbol{x}) = P^0_{loss}(\boldsymbol{x}_0) + \sum_{i=1}^{N_x} P^i_{loss}(\boldsymbol{x}_i) \tag{1}$$

where $P^0_{loss}(\boldsymbol{x}_0)$ is the term accounting for PCC interface losses, while $P^i_{loss}(\boldsymbol{x}_i)$, $i = 1, \ldots, N_x$ is the power loss of the i-th converter. The modeling of converter losses will be discussed in the next section. Regarding losses at PCC interface, a grid resistance R_g is assumed. To model loss terms it is convenient to define an extended vector $\boldsymbol{x}^e_i \in \mathbb{R}^{1\times 6}$ formed of $\boldsymbol{x}_i$ plus the extra element $I^+_{d,i}$:

$$\boldsymbol{x}^e_i = \left[I^+_{d,i}, \boldsymbol{x}_i\right] = \left[I^+_{d,i}, I^+_{q,i}, I^-_{d,i}, I^-_{q,i}, I^0_{d,i}, I^0_{q,i}\right] \tag{2}$$

Then, the losses on the grid resistance can be modeled as

$$P^0_{loss}(\boldsymbol{x}_0) = 3R_g \left\|\boldsymbol{x}^e_0\right\|^2 \tag{3}$$

where $\|\cdot\|$ denotes the 2-norm operator.

C. CONSTRAINTS

The considered microgrid is populated by uncontrollable units, which include loads (e.g., households, offices) and generators (e.g., wind turbines, photovoltaic panels), and by controllable units. In addition, the microgrid is tied to the main grid at the PCC. By the Kirchhoff current laws, the total contribution from the grid and the controllable units must sum to the net power absorption by the uncontrollable units $\boldsymbol{g} \in \mathbb{R}^{5\times 1}$:

$$\boldsymbol{g}^\top = \sum_{i=1}^{N_u} \boldsymbol{u}_i = \boldsymbol{x}_0 + \sum_{i=1}^{N_x} \boldsymbol{x}_i \tag{4}$$

Being $\boldsymbol{x} = [\boldsymbol{x}_0, \boldsymbol{x}_1, \ldots, \boldsymbol{x}_{N_x}]^\top$, it is possible to impose the constraint (4) as $\boldsymbol{G}\boldsymbol{x} - \boldsymbol{g} = \boldsymbol{0}$, with

$$\boldsymbol{G} = \left[\underbrace{\boldsymbol{I}_{5\times 5}, \boldsymbol{I}_{5\times 5}, \ldots, \boldsymbol{I}_{5\times 5}}_{(N_x+1) \text{ times}}\right] \tag{5}$$

where $\boldsymbol{I}_{5\times 5}$ is the identity matrix of size 5-by-5, being 5 the number of quantities contributed by each unit.

Converters have a maximum rated output current on each of its phases (i.e., phase a, b, and c). The algorithm shall not compute solutions where the reference values lead converters outside their safe operating region. Assuming a maximum output current on each phase $I_{\max,i}$ for the i-th converter, the following constraint should be met:

$$I^2_{a,i}, I^2_{b,i}, I^2_{c,i} \le I^2_{\max,i} \tag{6}$$

with $i = 1, \ldots, N_x$. The next step is to determine the value of $I^2_{a,i}, I^2_{b,i}, I^2_{c,i}$ from the vectors $\boldsymbol{x}^e_i$. By using suitable matrices $\boldsymbol{A}, \boldsymbol{B}, \boldsymbol{C} \in \mathbb{R}^{6\times 6}$, defined in (26) and derived in Appendix A, it yields:

$$I^2_{a,i} = \boldsymbol{x}^e_i \boldsymbol{A} \left(\boldsymbol{x}^e_i\right)^\top \; I^2_{b,i} = \boldsymbol{x}^e_i \boldsymbol{B} \left(\boldsymbol{x}^e_i\right)^\top \; I^2_{c,i} = \boldsymbol{x}^e_i \boldsymbol{C} \left(\boldsymbol{x}^e_i\right)^\top \tag{7}$$

To provide services to the upstream grid by exploiting the resources installed within the microgrid, additional constraints can be imposed, to achieve desired operating modes. In this article, the following additional operating modes are considered:

1) zero reactive power flow at the PCC;
2) perfectly balanced currents at the PCC.

Achieving 1) means that the first element of $\boldsymbol{x}_0$ is null, because that element represents the reactive power exchanged at the PCC. Achieving 2) means that the last four elements of $\boldsymbol{x}_0$ are null, since they are related to negative and zero sequence currents exchanged at the PCC. These two operating modes can be obtained by adding additional constraints. To selectively activate the operating modes, two boolean inputs σ_1, σ_2 are used, where $\sigma_i = 1$ means that the i-th condition is enabled, otherwise $\sigma_i = 0$.

The conditions 1) and 2) can be formulated as:

$$\boldsymbol{\sigma} \odot \boldsymbol{x}_0^\top = \boldsymbol{0} \tag{8}$$

where $\boldsymbol{\sigma} = [\sigma_1, \sigma_2, \sigma_2, \sigma_2, \sigma_2]^\top \in \mathbb{R}^{5\times 1}$, and $\odot$ indicates the element-wise multiplication (i.e., Hadamard product).

D. PROBLEM FORMULATION

Based on the presented modeling, the optimization problem can be formulated as:

$$\begin{cases} \min_{\boldsymbol{x}} & F(\boldsymbol{x}) \\ \text{s.t.} & \boldsymbol{G}\boldsymbol{x} - \boldsymbol{g} = \boldsymbol{0}; \\ & \boldsymbol{\sigma} \odot \boldsymbol{x}_0^\top = \boldsymbol{0}; \\ & \text{for } i = 1, \ldots, N_x: \\ & \boldsymbol{x}^e_i \boldsymbol{A} \left(\boldsymbol{x}^e_i\right)^\top \le I^2_{\max,i} \\ & \boldsymbol{x}^e_i \boldsymbol{B} \left(\boldsymbol{x}^e_i\right)^\top \le I^2_{\max,i} \\ & \boldsymbol{x}^e_i \boldsymbol{C} \left(\boldsymbol{x}^e_i\right)^\top \le I^2_{\max,i} \end{cases} \tag{9}$$

It is worth to remark that, assuming F be a convex function, whose actual expression and derivation are shown in Section IV, and being the constraints convex, the optimization problem (9) is convex [19].

III. SOLUTION METHOD

The solution method proposed herein is derived from *dual-ascent* technique. The resulting algorithm to solve the problem

in (9) is described in this section, while its actual implementation is discussed in Section V.

The dual-ascent method is an asymptotically optimal method to solve convex optimization problems using Lagrange multipliers [25], [26]. Dual-ascent is suitable for problems that exhibit a separable structure. In this case, the cost function is the sum of terms associated with different units, each depending solely on itself, so its application becomes natural.

Considering the problem in (9), its Lagrangian can be expressed as:

$$\begin{aligned}\mathcal{L}\{\boldsymbol{x}, \boldsymbol{\lambda}, \boldsymbol{v}, \boldsymbol{\mu}\} = F(\boldsymbol{x}) + \boldsymbol{\lambda}^\top (\boldsymbol{G}\boldsymbol{x} - \boldsymbol{g}) \\ + \boldsymbol{v}^\top \left(\boldsymbol{\sigma} \odot \boldsymbol{x}_0^\top\right) \\ + \boldsymbol{\mu}^\top (\boldsymbol{\Upsilon}_{abc} - \boldsymbol{\Upsilon}_{\max})\end{aligned} \tag{10}$$

where $\boldsymbol{\lambda} \in \mathbb{R}^{5\times 1}$, $\boldsymbol{\mu} \in \mathbb{R}^{3N_x\times 1}$, and $\boldsymbol{v} \in \mathbb{R}^{5\times 1}$ are column vectors containing Lagrange multipliers, and $\boldsymbol{\Upsilon}_{abc}, \boldsymbol{\Upsilon}_{\max} \in \mathbb{R}^{3N_x\times 1}$ are the vectors containing the squares of the per-phase currents and maximum currents of all controllable units:

$$\boldsymbol{\Upsilon}_{abc} = \begin{bmatrix} I_{a,1}^2 \\ I_{b,1}^2 \\ I_{c,1}^2 \\ \vdots \\ I_{a,N_x}^2 \\ I_{b,N_x}^2 \\ I_{c,N_x}^2 \end{bmatrix}; \quad \boldsymbol{\Upsilon}_{\max} = \begin{bmatrix} I_{\max,1}^2 \\ I_{\max,1}^2 \\ I_{\max,1}^2 \\ \vdots \\ I_{\max,N_x}^2 \\ I_{\max,N_x}^2 \\ I_{\max,N_x}^2 \end{bmatrix} \tag{11}$$

The dual-ascent is traditionally implemented by iteratively updating the solution $\boldsymbol{x}$ as follows:

$$\boldsymbol{x}(k+1) = \arg\min_{\boldsymbol{x}} \mathcal{L}\{\boldsymbol{x}, \boldsymbol{\lambda}(k), \boldsymbol{v}(k), \boldsymbol{\mu}(k)\} \tag{12}$$

When the solution exists in closed form, (12) can be solved as $\nabla_{\boldsymbol{x}}\mathcal{L} = 0$, as done in [21]. If a closed-form solution is not available, other strategies should be applied. A simplex method (see, e.g., [27]) is employed in [22] for solving (12); the drawback of that approach is the computation burden of the simplex algorithm's iterative nature, involved in each dual-ascent iteration.

Differently, it is worth noting that, even if the solution of $\nabla\mathcal{L}_{\boldsymbol{x}} = 0$ can not be computed, it is still possible to compute the expression of $\nabla_{\boldsymbol{x}}\mathcal{L}$. By exploiting the values of $\nabla_{\boldsymbol{x}}\mathcal{L}$, the update of $\boldsymbol{x}(k+1)$ can be performed by taking a finite number of steps in the opposite direction of $\nabla_{\boldsymbol{x}}\mathcal{L}$ with a fixed step-size. A single-step update is performed herein, obtaining:

$$\boldsymbol{x}(k+1) = \boldsymbol{x}(k) - \alpha\nabla_{\boldsymbol{x}}\mathcal{L}\{\boldsymbol{x}(k), \boldsymbol{\lambda}(k), \boldsymbol{v}(k), \boldsymbol{\mu}(k)\} \tag{13}$$

where α is the step size. Equation (13) resembles the updating step of the primal variable implemented in the primal-dual algorithm [28].

The update of the Lagrange multipliers for equality constraints is performed as:

$$\begin{cases}\boldsymbol{\lambda}(k+1) = \boldsymbol{\lambda}(k) + \beta\left[\boldsymbol{G}\boldsymbol{x}(k+1) - \boldsymbol{g}\right] \\ \boldsymbol{v}(k+1) = \boldsymbol{v}(k) + \delta\left[\boldsymbol{\sigma}(k) \odot \boldsymbol{x}_0^\top(k+1)\right]\end{cases} \tag{14}$$

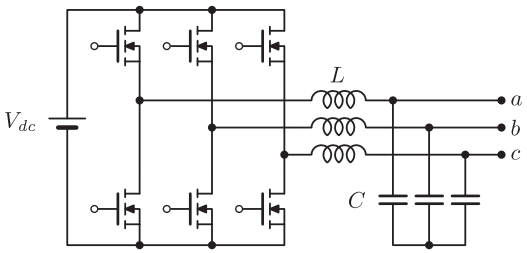

FIGURE 2. Topology considered for the power losses characterization.

where β, δ are the step sizes of the update. By Karush-Kuhn-Tucker (KKT) conditions, the update of the Lagrange multipliers related to inequality constraints has to be performed by setting 0 as their lower bound:

$$\boldsymbol{\mu}(k+1) = \min\{0,\ \boldsymbol{\mu}(k) + \gamma\left[\boldsymbol{\Upsilon}_{abc} - \boldsymbol{\Upsilon}_{\max}\right]\} \tag{15}$$

where γ is the step size.

After the considerations done above, the $(k+1)$-th iteration of the primal-dual algorithm can be performed as:

$$\begin{cases}\boldsymbol{x}(k+1) = \boldsymbol{x}(k) - \alpha\nabla_{\boldsymbol{x}}\mathcal{L}\{\boldsymbol{x}(k), \boldsymbol{\lambda}(k), \boldsymbol{v}(k), \boldsymbol{\mu}(k)\} \\ \boldsymbol{\lambda}(k+1) = \boldsymbol{\lambda}(k) + \beta\left[\boldsymbol{G}\boldsymbol{x}(k+1) - \boldsymbol{g}\right] \\ \boldsymbol{v}(k+1) = \boldsymbol{v}(k) + \delta\left[\boldsymbol{\sigma}(k) \odot \boldsymbol{x}_0^\top(k+1)\right] \\ \boldsymbol{\mu}(k+1) = \min\{0,\ \boldsymbol{\mu}(k) + \gamma\left[\boldsymbol{\Upsilon}_{abc} - \boldsymbol{\Upsilon}_{\max}\right]\}\end{cases} \tag{16}$$

IV. COST FUNCTION BASED ON CONVERTER LOSSES

The power losses of a typical three-phase half-bridge topology have been characterized with respect to the operating conditions.

For a single-phase converter, power losses can be modeled as a quadratic function of the rms output current [21]:

$$P_{loss}^{1\phi} = a \cdot I_{rms}^2 + b \cdot I_{rms} + c \tag{17}$$

The topology considered herein is displayed in Fig 2.

The characterization for the three-phase converter aimed to find a fitting function f such that losses can be expressed as:

$$P_{loss}^{i} = f\left(I_{d,i}^+, I_{q,i}^+, I_{d,i}^-, I_{q,i}^-, I_{d,i}^0, I_{q,i}^0\right) \tag{18}$$

namely, as a function of dq components of symmetric sequences.

A. OVERVIEW OF THE EXPERIMENTAL SETUP

A 3 kW experimental rapid prototyping system [29] has been employed to perform the characterization of the losses. Fig. 2 shows the topology considered. A Dewesoft Sirius-i data acquisition system is used to acquire the data and perform the computation of power loss, by means of the dedicated software run on a desktop PC. A 30 kW Cinergia grid emulator is employed to emulate the ac side, while a Keysight RP7962 A is used as the dc source for the converter under test. A schematic representation of the setup is shown in Fig. 3.

B. POWER LOSSES MEASUREMENT

Power losses have been measured on the converter under test in about 4500 different operating points $[I_d^+, I_q^+, I_d^-, I_q^-] \in \mathbb{R}^4$. These points are determined by uniformly sampling $\mathbb{R}^4$ over the nominal converter ratings, removing all the points

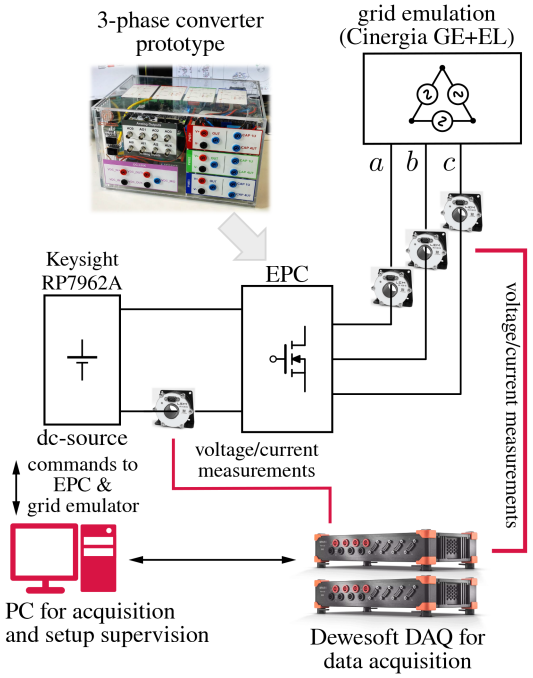

FIGURE 3. Schematic representation of the employed setup.

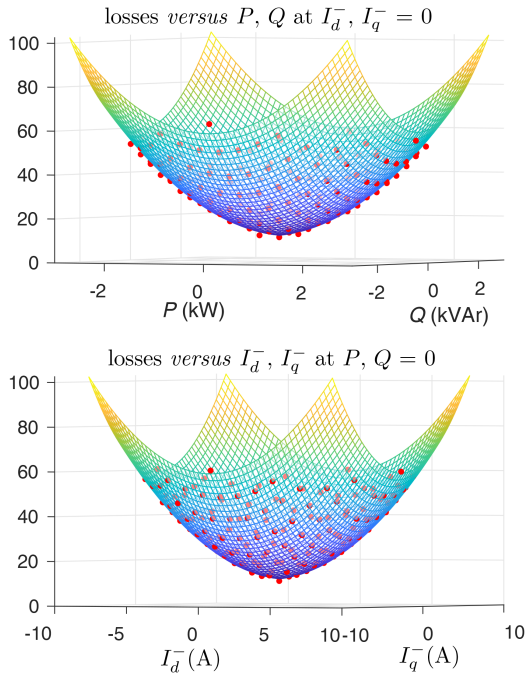

FIGURE 4. Experimental data (red dots) correctly fitted by the considered loss function (19).

in which at least one of the per-phase currents exceeds the maximum value allowed. When steady state is reached, the converter losses are measured.

In light of the analysis done in [21], the following fitting function is considered:

$$f(|I|) = a \cdot |I|^2 + b \cdot |I| + c \tag{19}$$

where $|I|^2 = |I_d^+|^2 + |I_q^+|^2 + |I_d^-|^2 + |I_q^-|^2$ is three-phase current mean-square value. The chosen function (19) correctly fits the measured data, as shown in Fig. 4.

The expression in (19) shows the dependence of power losses on the rms three-phase current. Generalization of (19) may be possible considering also zero-sequence components. This latter case is included in this work assuming the model:

$$P_{loss}^i(I) = a_i \cdot |I_i|^2 + b_i \cdot |I_i| + c_i \tag{20}$$

where $|I_i|^2 = |I_{d,i}^+|^2 + |I_{q,i}^+|^2 + |I_{d,i}^-|^2 + |I_{q,i}^-|^2 + |I_{d,i}^0|^2 + |I_{q,i}^0|^2$.

V. ALGORITHM IMPLEMENTATION

A flowchart of the algorithm is shown in Fig. 5. At the beginning, each controllable electronic power converter (EPC) sends to the MC the coefficients of its cost function a_i, b_i, c_i and the current operating point $\boldsymbol{x}_i^e$. The MC also receives the measured quantities at the PCC $\boldsymbol{x}_0^e$. It is assumed that the MC knows the maximum per-phase current $I_{\max,i}$ for each EPC.

As in (4), the MC can compute the value of $\boldsymbol{g}$ based solely on the operating points of the controllable units:

$$\boldsymbol{g}^\top = \boldsymbol{x}_0 + \sum_{i=1}^{N_x} \boldsymbol{x}_i \tag{21}$$

To compute the optimal solution, a fixed number of iterations $N_k = 1000$ is chosen, in which (16) is run. When N_k

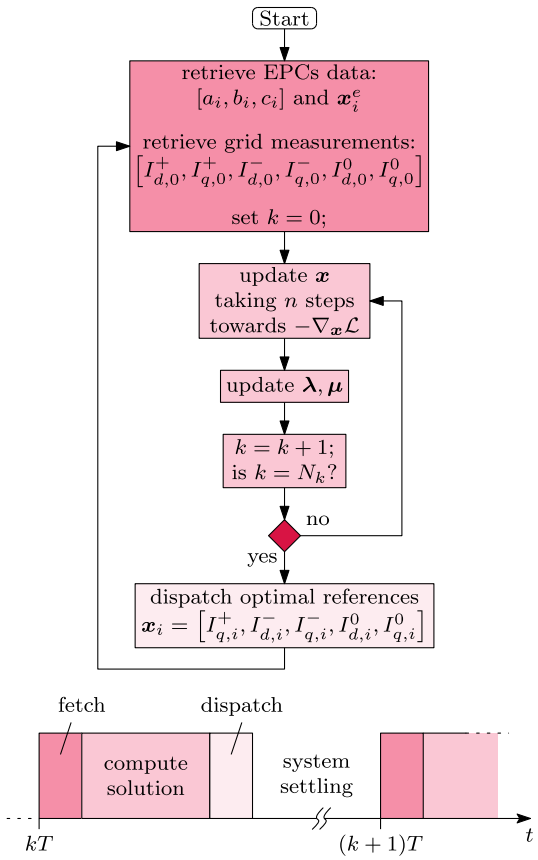

FIGURE 5. Flowchart of the proposed primal-dual based coordination algorithm. Temporal sequence of executed tasks represented on the bottom.

Algorithm 1: Pseudocode of the Proposed Approach, Illustrated in Fig. 5.

Start: go to **Fetch**;
Fetch:
  Receive $\boldsymbol{x}_i^e$ and a_i, b_i, c_i from EPCs;
  Receive $\boldsymbol{x}_0^e$ from PCC;
  Initialize $\boldsymbol{x}$ to system current state;
  Compute $\boldsymbol{g}$ using (21);
  $k \leftarrow 0$;
  go to **Compute**;
Compute:
  Update $\boldsymbol{x}$ using (13);
  Update $\boldsymbol{\lambda}$ using (14);
  Compute $\boldsymbol{\Upsilon}_{abc}$ using (7) and (11);
  Update $\boldsymbol{\mu}$ using (15);
  $k \leftarrow k+1$;
  if $k < N_x$: go to **Compute**;
  else: go to **Dispatch**;
Dispatch:
  Send optimal reference points to EPCs;
  while settling *not* reached: wait;
  go to **Fetch**;

is reached, the current solution $\boldsymbol{x}(k)$ is dispatched as reference operating point for the EPCs. Then the algorithm is iterated. To better clarify all the steps involved more in detail, the pseudocode is shown in Algorithm 1.

As mentioned in Section II, the approach assumes low bandwidth communication links between each controllable unit and the microgrid controller where the optimization algorithm is implemented. The execution rate of the algorithm is set to 6 executions per hour, which is suitable for the considered power profiles variation. Remarkably, the computational burden of such an algorithm allows a much higher execution rate on modern digital controllers, as further elaborated in Section VI. This allows sufficient time for the controller to receive the data from controllable units, compute and dispatch the new optimal solution, and allow converters to reach the new operating point. Remarkably, each execution is a different optimization problem. This allows interrupt-based variable-rate implementation, where the MC executes the optimization algorithm as soon as all the new data is received. Converters can manage their own settling time by sending the data only after their transient is completed.

VI. APPLICATION EXAMPLE

To show the effectiveness of the proposal, the low-voltage microgrid benchmark proposed by Cigre [30] is taken as a benchmark, and the proposed method is tested in a scenario where the units in the grid are provided with a varying power profile along 24 hours.

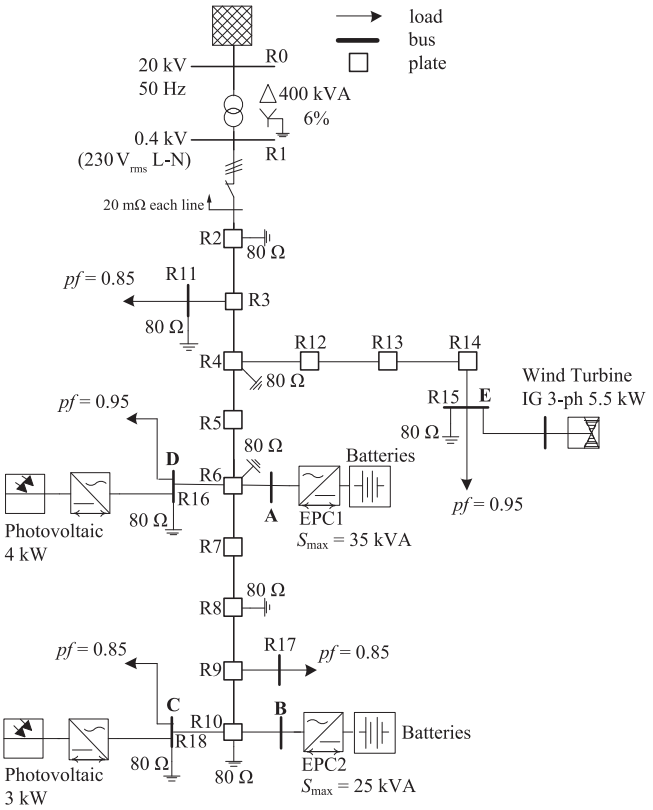

Converters Cost Functions

Grid resistance	R_g	20 mΩ
EPC1 cost function	$[a_1, b_1, c_1]$	$[0.0411, 4.46, 123]$
EPC2 cost function	$[a_2, b_2, c_2]$	$[0.0797, 6.80, 114]$

FIGURE 6. Considered microgrid benchmark, adapted from [30]. The table on the bottom illustrates the cost functions for the controllable units.

A. BENCHMARK DESCRIPTION

The microgrid, shown in Fig. 6, is composed of unbalanced loads, wind turbines, photovoltaic panels, and energy storage systems (batteries). In the considered tests, only battery-sourced converters EPC1 and EPC2 are considered as dispatchable, so the algorithm runs optimizing their operating point. Loads and non-controllable converters are considered non-controllable units.

The loads and generators of the microgrid are considered with a variable power profile, along 24 hours. The photovoltaic sources, at nodes C and D, and wind turbines, at node E, in Fig. 6, have power profiles obtained from real data [31] and [32], respectively, with nominal peak power as indicated in the same figure.

The loads in the microgrid are buildings, either residential or commercial. In particular, the loads at nodes D and E represent offices with three-phase connection, while each phase of all the other loads represents houses, each having an independent randomly generated power profile, which causes unbalanced power absorption considered the three-phase network. Load absorptions from offices and houses are generated using a Matlab-based app [33]. The nodes D and E have a

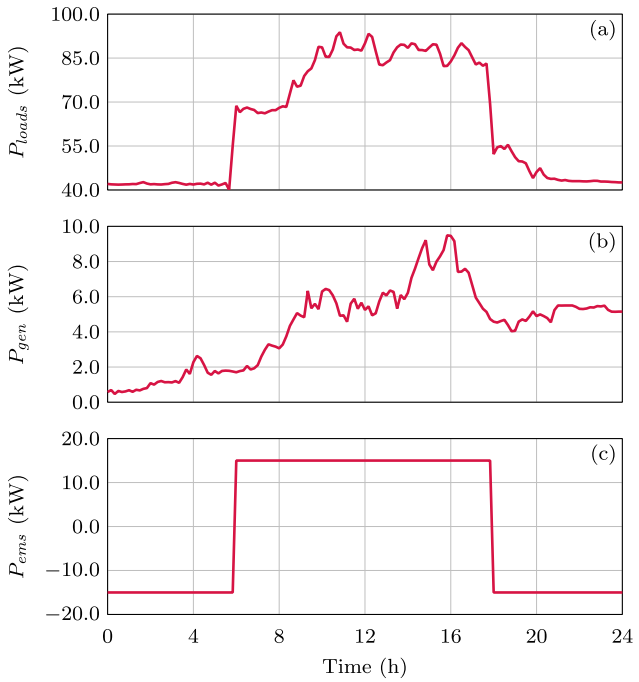

FIGURE 7. Aggregated active power profiles of units in the considered microgrid: (a) total power absorbed by the loads; (b) total power generated by renewable sources; (c) active output power of EPC1 and EPC2.

power factor equal to 0.95, while all the other loads have a power equal to 0.85. Distribution lines are made of six different types of conductors, with R/X-ratio ranging from 1.76 to 7.48; the line impedance values are detailed in [30]. Finally, the active power of EPC1 and EPC2 are assumed to be managed by an energy management system, which supplies 15 kW active power during peak demand (i.e., from 6 a.m. to 6 p.m.) and recharges the batteries at 15 kW for the remaining time. The total power is then shared among EPC1 and EPC2 proportionally to their nominal powers.

The profiles for the various units in the microgrid are reported in Fig. 7, where P_{loads} is the total power absorbed by the loads (i.e., offices and houses), P_{gen} is the generated power from PV panels and wind turbine, and P_{ems} is the total active power output of EPC1 and EPC2.

The coefficients a_i, b_i, c_i for controllable EPCs are derived from the efficiency curves versus percentage output power of two commercially available inverters, namely [34] for EPC1 and [35] for EPC2. From the efficiency curves, the curve of power loss with respect to three-phase rms current is derived, and fitted using (20) to obtain a_i, b_i, c_i. Fig. 8 shows the efficiency data and the fitting curves. A 20 mΩ resistance is considered on each phase at the PCC to model grid losses.

B. TEST RESULTS

Four different scenarios are considered and compared in the following:

- *Case 1*: algorithm disabled, controllable EPCs only exchange active power as in Fig. 7(c);
- *Case 2*: the algorithm provides optimal reference values to controllable EPCs;

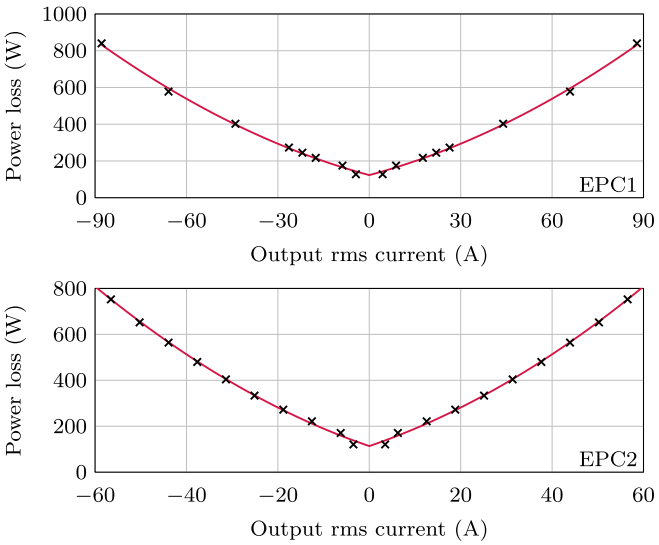

FIGURE 8. Efficiency curves (black crosses) from data reported in [34] and [35], respectively, and fitting curves (red curves) from (20).

- *Case 3*: the algorithm provides optimal references to achieve balanced currents at PCC;
- *Case 4*: the algorithm provides optimal references to achieve balanced currents and zero reactive-power flow at PCC.

Fig. 9 collects and allows the comparison of the results from the different test cases considered. To compute an unbalance factor that accounts for both negative and zero sequence currents, the following formula is used:

$$UF_{\%} = \frac{\sqrt{|I^-|^2 + |I^0|^2}}{|I^+|} \cdot 100 \tag{22}$$

The power factor is instead computed as $PF = P/S$.

The results show that the most efficient operation is achieved in **Case 2**, as expected. The power loss is reduced by more than 5% with respect to **Case 1**, during peak demand. It is worth remarking that the efficiency gains depend on the actual microgrid structure and operating conditions, and may vary based on the compensation effort required to the converters. In this case, the loads with higher power absorption present a higher power factor, namely, 0.95. Of course, if such a PF is decreased, then a greater reduction in losses is expected with respect to **Case 1**. **Case 2** also leads to improvements in power factor and PCC current unbalance factor, because now part of the reactive power and unbalanced currents are provided by EPC1 and EPC2, thanks to the coordination algorithm.

Case 3 considers the service of imposing balanced current flow at PCC, by means of the constraints presented in Section II-II-C. This setting of the control algorithm achieves perfectly balanced currents at the PCC, while limiting the power loss.

Finally, operation in **Case 4** allows to achieve unitary power factor at the PCC, with PCC currents perfectly balanced. This operation mode engages the distributed controllable units with

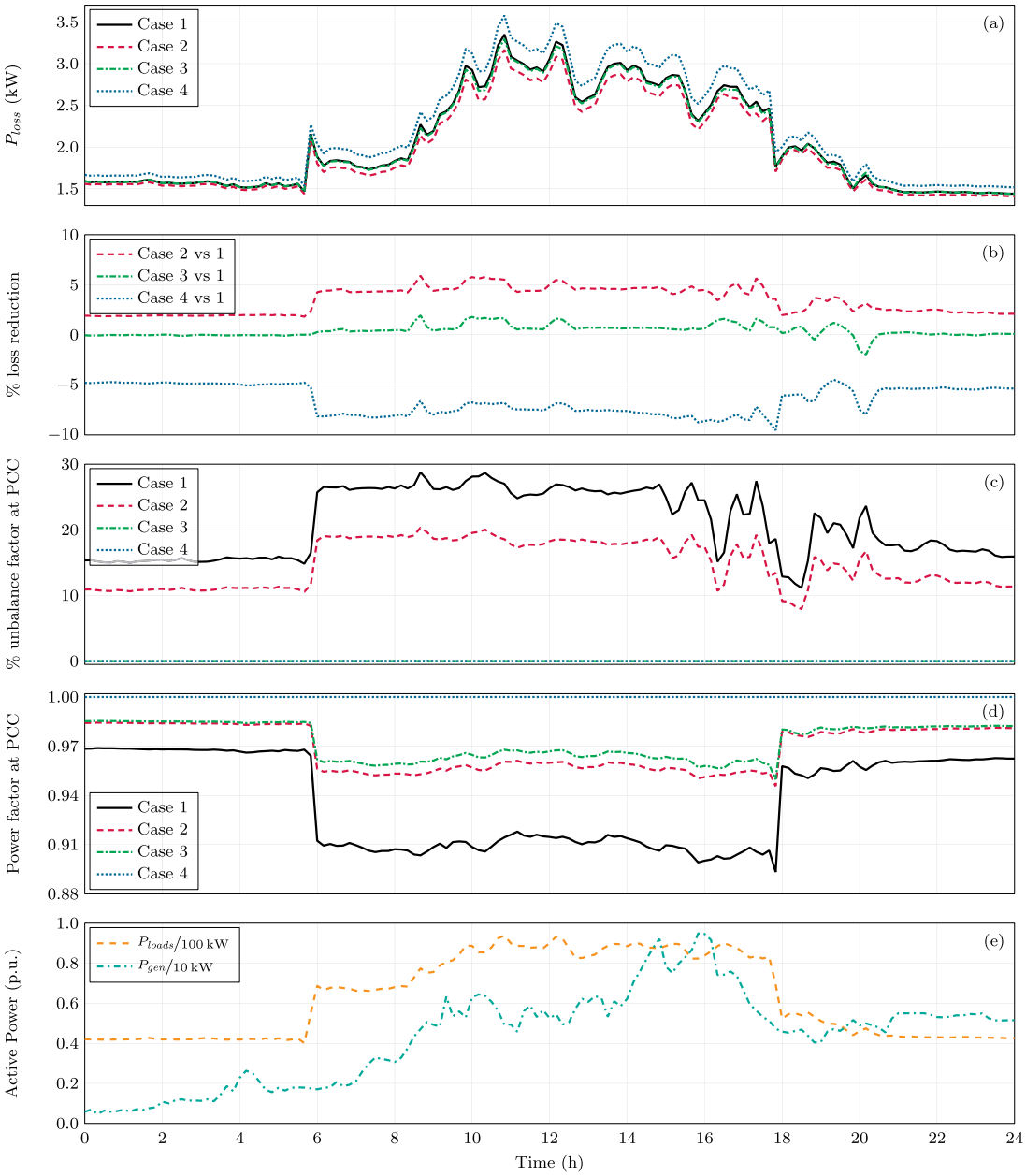

FIGURE 9. Simulation results: (a) total power loss of the system; (b) percentage loss reduction with respect to Case 1; (c) unbalance factor of currents at PCC; (d) power factor at PCC; (e) power demand and generation in the microgrid.

a higher effort, which brings to a loss increase with respect to **Case 1**. In fact, this mode of operation requires EPC1 and EPC2 to supply the full unbalanced currents and reactive power required within the microgrid.

C. ALGORITHM PERFORMANCE

The algorithm's convergence performance has been assessed to verify its effectiveness. The assessment encompasses all the algorithm executions in all four cases considered.

Fig. 10 shows the result. On the x-axis, the plot reports the number of iterations, with $k \in [0, 1000]$; on the y-axis, the plot reports the percentage of setpoints $\boldsymbol{x}$ that, after k iterations, are closer than a threshold ϵ_t to the ideal final solution $\boldsymbol{x}^*$ (i.e., the convergence value), over all the executions of the considered cases along the 24 h. The threshold ϵ_t is a given relative-error, computed as the 2-norm of the difference between the ideal final solution and the solution found after k iterations, divided by the 2-norm of the ideal final solution:

$$\varepsilon_{\%} = \frac{\|\boldsymbol{x}(k) - \boldsymbol{x}^*\|_2}{\|\boldsymbol{x}^*\|_2} \cdot 100 \tag{23}$$

Several thresholds are considered herein, namely, 5%, 1%, and 0.1%. Notably, after 200 iterations, the error is always below 5%, while after less than 400 iterations the error is always below 1%. It takes slightly more than 600 iterations to keep the error below 0.1%.

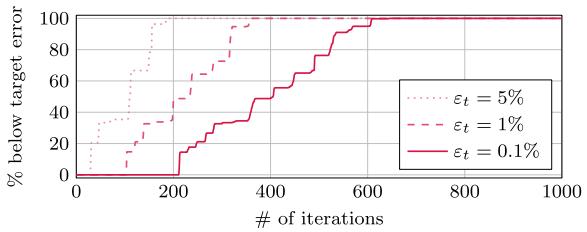

FIGURE 10. Convergence performance of the proposed algorithm. Percentage of intermediate solutions, after the indicated # of iterations, that are closer than the threshold ϵ_t to the ideal final solution (i.e., the convergence value).

Moreover, the computational effort needed to run the algorithm has also been evaluated. Specifically, the proposed algorithm has been implemented in an Imperix B-Board Pro^{TM} control board [36], which embeds two 1 GHz ARM CPUs. The real-time execution rate has been set to 50 kHz, and is responsible for the local control task of regulating the converter output quantities by the grid-forming control method presented in [37], while the proposed algorithm runs at 1 Hz. The timing analysis tool of the control platform reports an average usage of the controller of 39.94%, with a peak of 47.23%. This shows the method described herein can be, for instance, executed by the control board of one of the converters present in the considered microgrid alongside the local control tasks, without the need for a dedicated centralized control unit. Still, in applications, dedicated microgrid controllers may be available, as foreseen by relevant standards [38], and employed for running the optimization algorithm.

VII. CONCLUSION

The approach presented in this paper optimizes the provision of unbalanced and reactive currents, encompassing grid and converter losses. The considered topology has been experimentally characterized, to derive a model for its power losses with respect to the operating conditions. An optimization problem has been formulated as a Lagrange multipliers problem, and it has been solved using a proposed algorithm based on the primal-dual method. Simulations are carried out on a modified Cigre benchmark microgrid, considering the typical power profiles of its units along 24 hours, proving the effectiveness of the proposed approach in mitigating the power losses of the system and in compensating unbalanced and reactive currents at the PCC. In a microgrid control hierarchy, the proposal can implement a control layer receiving input from other higher-level economic policies that define ancillary service setpoints and energy transactions and providing references to lower-level inner and primary controllers (e.g., droop-like controllers) of distributed electronic converters. Being able to effectively deal with quadratic (or even pseudo-quadratic, as in this case) cost functions, the proposed method can be an effective solution in a very wide class of different problems. Moreover, with its light computational cost, it may not even need a dedicated controller carrying out its control tasks solely, but could be run alongside other control tasks on a local controller.

APPENDIX
DQ SYMMETRICAL-COMPONENTS TO PER-PHASE RMS CURRENTS

The matrices $\boldsymbol{A}, \boldsymbol{B}, \boldsymbol{C}$ used in (7) allow to obtain the squared absolute value of per-phase currents, namely $I_{a,i}^2, I_{b,i}^2, I_{c,i}^2$, from the vector $\boldsymbol{x}_i^e = [I_{d,i}^+, I_{q,i}^+, I_{d,i}^-, I_{q,i}^-, I_{d,i}^0, I_{q,i}^0]$. The derivation is simple but involves some calculations.

From symmetrical components, *abc* components can be obtained as:

$$\begin{bmatrix} \underline{I}_a \\ \underline{I}_b \\ \underline{I}_c \end{bmatrix} = \begin{bmatrix} 1 & 1 & 1 \\ \underline{a}^2 & \underline{a} & 1 \\ \underline{a} & \underline{a}^2 & 1 \end{bmatrix} \begin{bmatrix} \underline{I}^+ \\ \underline{I}^- \\ \underline{I}^0 \end{bmatrix}; \quad \underline{a} = e^{j\frac{2\pi}{3}} \tag{24}$$

where underline indicates complex quantities. By decomposing the symmetrical components in their dq components, from (24) one obtains:

$$\begin{aligned}
\underline{I}_a &= \underline{I}^+ + \underline{I}^- + \underline{I}^0 = I_d^+ + I_d^- + I_d^0 + j\left(I_q^+ + I_q^- + I_q^0\right) \\
\underline{I}_b &= \underline{a}^2\underline{I}^+ + \underline{a}\,\underline{I}^- + \underline{I}^0 \\
&= -\frac{1}{2}I_d^+ + \frac{\sqrt{3}}{2}I_q^+ - \frac{1}{2}I_d^- - \frac{\sqrt{3}}{2}I_q^- + I_d^0 \\
&\quad + j\left(-\frac{\sqrt{3}}{2}I_d^+ - \frac{1}{2}I_q^+ + \frac{\sqrt{3}}{2}I_d^- - \frac{1}{2}I_q^- + I_q^0\right) \\
\underline{I}_c &= \underline{a}\,\underline{I}^+ + \underline{a}^2\underline{I}^- + \underline{I}^0 \\
&= \frac{1}{2}I_d^+ - \frac{\sqrt{3}}{2}I_q^+ - \frac{1}{2}I_d^- + \frac{\sqrt{3}}{2}I_q^- + I_d^0 \\
&\quad + j\left(\frac{\sqrt{3}}{2}I_d^+ - \frac{1}{2}I_q^+ - \frac{\sqrt{3}}{2}I_d^- - \frac{1}{2}I_q^- + I_q^0\right)
\end{aligned}$$

Taking the squared absolute value of $\underline{I}_a, \underline{I}_b, \underline{I}_c$ one obtains the following expressions:

$$\begin{aligned}
I_a^2 = {} & \left(I_d^+\right)^2 + \left(I_q^+\right)^2 + \left(I_d^-\right)^2 + \left(I_q^-\right)^2 + \left(I_d^0\right)^2 + \left(I_q^0\right)^2 \\
& + 2I_d^+I_d^- + 2I_d^+I_d^0 + 2I_q^+I_q^- + 2I_q^+I_q^0 + 2I_d^-I_d^0 + 2I_q^-I_q^0 \\
I_b^2 = {} & \left(I_d^+\right)^2 + \left(I_q^+\right)^2 + \left(I_d^-\right)^2 + \left(I_q^-\right)^2 + \left(I_d^0\right)^2 + \left(I_q^0\right)^2 \\
& - I_d^+I_d^- - I_d^+I_d^0 - I_q^+I_q^- - I_q^+I_q^0 - I_d^-I_d^0 - I_q^-I_q^0 \\
& + \sqrt{3}I_d^+I_q^- - \sqrt{3}I_d^+I_q^0 - \sqrt{3}I_q^+I_d^- - \sqrt{3}I_q^+I_d^0 \\
& + \sqrt{3} + I_d^-I_q^0 - \sqrt{3}I_q^-I_d^0 \\
I_c^2 = {} & \left(I_d^+\right)^2 + \left(I_q^+\right)^2 + \left(I_d^-\right)^2 + \left(I_q^-\right)^2 + \left(I_d^0\right)^2 + \left(I_q^0\right)^2 \\
& - I_d^+I_d^- - I_d^+I_d^0 - I_q^+I_q^- - I_q^+I_q^0 - I_d^-I_d^0 - I_q^-I_q^0 + \\
& - \sqrt{3}I_d^+I_q^- + \sqrt{3}I_d^+I_q^0 + \sqrt{3}I_q^+I_d^- + \sqrt{3}I_q^+I_d^0 \\
& - \sqrt{3} - I_d^-I_q^0 + \sqrt{3}I_q^-I_d^0
\end{aligned}$$

For the i-th controllable unit, the expressions of I_a^2, I_b^2, I_c^2 can be derived by

$$I_{x,i}^2 = \boldsymbol{x}_i^e \boldsymbol{X} \left(\boldsymbol{x}_i^e\right)^\top; \quad \boldsymbol{X} = \boldsymbol{A}, \boldsymbol{B}, \boldsymbol{C} \tag{25}$$

From (25) one can easily see that the squared terms in the expressions I_a^2, I_b^2, I_c^2 are obtained having 1 in the main diagonal of the matrices $\boldsymbol{A}, \boldsymbol{B}, \boldsymbol{C}$, while the other monomials are obtained by placing half of their coefficients in the related rows and columns of the matrix, obtaining $\boldsymbol{X} = \boldsymbol{X}^\top$. The matrices are, therefore:

$$\boldsymbol{A} = \begin{bmatrix} 1 & 0 & 1 & 0 & 1 & 0 \\ 0 & 1 & 0 & 1 & 0 & 1 \\ 1 & 0 & 1 & 0 & 1 & 0 \\ 0 & 1 & 0 & 1 & 0 & 1 \\ 1 & 0 & 1 & 0 & 1 & 0 \\ 0 & 1 & 0 & 1 & 0 & 1 \end{bmatrix}$$

$$\boldsymbol{B} = \begin{bmatrix} 1 & 0 & \frac{1}{2} & \frac{\sqrt{3}}{2} & \frac{1}{2} & -\frac{\sqrt{3}}{2} \\ 0 & 1 & -\frac{\sqrt{3}}{2} & \frac{1}{2} & \frac{\sqrt{3}}{2} & \frac{1}{2} \\ \frac{1}{2} & -\frac{\sqrt{3}}{2} & 1 & 0 & \frac{1}{2} & \frac{\sqrt{3}}{2} \\ \frac{\sqrt{3}}{2} & \frac{1}{2} & 0 & 1 & -\frac{\sqrt{3}}{2} & \frac{1}{2} \\ \frac{1}{2} & \frac{\sqrt{3}}{2} & \frac{1}{2} & -\frac{\sqrt{3}}{2} & 1 & 0 \\ -\frac{\sqrt{3}}{2} & \frac{1}{2} & \frac{\sqrt{3}}{2} & \frac{1}{2} & 0 & 1 \end{bmatrix}$$

$$\boldsymbol{C} = \begin{bmatrix} 1 & 0 & \frac{1}{2} & -\frac{\sqrt{3}}{2} & \frac{1}{2} & \frac{\sqrt{3}}{2} \\ 0 & 1 & \frac{\sqrt{3}}{2} & \frac{1}{2} & -\frac{\sqrt{3}}{2} & \frac{1}{2} \\ \frac{1}{2} & \frac{\sqrt{3}}{2} & 1 & 0 & \frac{1}{2} & -\frac{\sqrt{3}}{2} \\ -\frac{\sqrt{3}}{2} & \frac{1}{2} & 0 & 1 & \frac{\sqrt{3}}{2} & \frac{1}{2} \\ \frac{1}{2} & -\frac{\sqrt{3}}{2} & \frac{1}{2} & \frac{\sqrt{3}}{2} & 1 & 0 \\ \frac{\sqrt{3}}{2} & \frac{1}{2} & -\frac{\sqrt{3}}{2} & \frac{1}{2} & 0 & 1 \end{bmatrix} \tag{26}$$

ACKNOWLEDGMENT

This manuscript reflects only the authors' views and opinions, neither the European Union nor the European Commission can be considered responsible for them.

REFERENCES

[1] T. Caldognetto, H. Abedini, and P. Mattavelli, "A per-phase power controller for smooth transitions to islanded operation," *IEEE Open J. Power Electron.*, vol. 2, pp. 636–646, 2021.

[2] A. Lauri, T. Caldognetto, D. Biadene, H. Abedini, and P. Mattavelli, "Per-phase power controller for smooth islanded transitions in three-phase three-wire systems," *Energies*, vol. 16, no. 2, Jan. 2023, Art. no. 672.

[3] R. V. Ferreira, S. M. Silva, and D. I. Brandao, "Positive–negative sequence synchronverter for unbalanced voltage in AC grids," *J Control Autom. Elect. Syst.*, vol. 32, no. 3, pp. 711–720, Jun. 2021.

[4] R. Ghosh, N. R. Tummuru, and B. S. Rajpurohit, "A new virtual oscillator-based grid-forming controller with decoupled control over individual phases and improved performance of unbalanced fault ride-through," *IEEE Trans. Ind. Electron.*, vol. 70, no. 12, pp. 12465–12474, Dec. 2023.

[5] E. Espina, M. Espinoza, and R. Cárdenas, "Active power angle droop control per phase for unbalanced 4-wire microgrids," in *Proc. IEEE South. Power Electron. Conf.*, 2017, pp. 1–6.

[6] Y. Wu, J. Shi, G. J. Lim, L. Fan, and A. Molavi, "Optimal management of transactive distribution electricity markets with co-optimized bidirectional energy and ancillary service exchanges," *IEEE Trans. Smart Grid*, vol. 11, no. 6, pp. 4650–4661, Nov. 2020.

[7] S. F. Contreras, C. A. Cortes, and J. M. A. Myrzik, "Optimal microgrid planning for enhancing ancillary service provision," *J. Mod. Power Syst. Clean Energy*, vol. 7, no. 4, pp. 862–875, Jul. 2019.

[8] T. M. Blasi, T. S. P. Fernandes, A. R. Aoki, and F. H. Tabarro, "Multi-period optimum power flow for active distribution networks with provisioning of ancillary services," *IEEE Access*, vol. 9, pp. 110371–110395, 2021.

[9] I. G. Marneris et al., "Optimal participation of RES aggregators in energy and ancillary services markets," *IEEE Trans. Ind. Appl.*, vol. 59, no. 1, pp. 232–243, Jan./Feb. 2023.

[10] C. Opathella, A. Elkasrawy, A. A. Mohamed, and B. Venkatesh, "Optimal scheduling of merchant-owned energy storage systems with multiple ancillary services," *IEEE Open Access J. Power Energy*, vol. 7, pp. 31–40, 2020.

[11] A. Maneesha and K. S. Swarup, "Stochastic optimal bidding strategy for energy and ancillary services in microgrid," *IEEE Trans. Ind. Appl.*, vol. 57, no. 6, pp. 5698–5705, Nov./Dec. 2021.

[12] S. Karagiannopoulos, J. Gallmann, M. G. Vayá, P. Aristidou, and G. Hug, "Active distribution grids offering ancillary services in islanded and grid-connected mode," *IEEE Trans. Smart Grid*, vol. 11, no. 1, pp. 623–633, Jan. 2020.

[13] Y. Cao, Y. Tan, C. Li, and C. Rehtanz, "Chance-constrained optimization-based unbalanced optimal power flow for radial distribution networks," *IEEE Trans. Power Del.*, vol. 28, no. 3, pp. 1855–1864, Jul. 2013.

[14] A. Nikpour, A. Nateghi, and M. Shafie-Khah, "Stochastic-risk based approach for microgrid participation in joint active, reactive, and ancillary services markets considering demand response," *IEEE Open Access J. Power Energy*, vol. 10, pp. 2–13, 2023.

[15] L. R. Araujo, D. R. R. Penido, S. Carneiro, and J. L. R. Pereira, "A three-phase optimal power-flow algorithm to mitigate voltage unbalance," *IEEE Trans. Power Del.*, vol. 28, no. 4, pp. 2394–2402, Oct. 2013.

[16] D. M. Ferreira, D. I. Brandao, G. Bergna-Diaz, E. Tedeschi, and S. M. Silva, "Distributed control strategy for low-voltage three-phase four-wire microgrids: Consensus power-based control," *IEEE Trans. Smart Grid*, vol. 12, no. 4, pp. 3215–3231, Jul. 2021.

[17] S. Roy Ghatak, S. Sannigrahi, and P. Acharjee, "Multiobjective framework for optimal integration of solar energy source in three-phase unbalanced distribution network," *IEEE Trans. Ind. Appl.*, vol. 56, no. 3, pp. 3068–3078, May/Jun. 2020.

[18] L. Meng, F. Tang, M. Savaghebi, J. C. Vasquez, and J. M. Guerrero, "Tertiary control of voltage unbalance compensation for optimal power quality in islanded microgrids," *IEEE Trans. Energy Convers.*, vol. 29, no. 4, pp. 802–815, Dec. 2014.

[19] S. P. Boyd and L. Vandenberghe, *Convex Optimization*. Cambridge, U.K.: Cambridge Univ. Press, 2023.

[20] Y. Jiang, Y. Yang, S.-C. Tan, and S.-Y. R. Hui, "Lagrange multiplier-based optimization control for distribution power loss minimization of islanded three-phase AC microgrids," in *Proc. IEEE IAS Ind. Commercial Power Syst. Asia*, 2021, pp. 489–494.

[21] Y. Jiang and Y. Yang, "Dual ascent algorithm-based improved droop control for efficient operation of AC microgrid," *Front. Electron.*, vol. 3, 2022, Art. no. 926865.

[22] A. Lauri, T. Caldognetto, R. Carli, D. Biadene, and P. Mattavelli, "Dual-ascent optimization for the provision of ancillary services in three-phase low-voltage microgrids," in *Proc. IEEE 8th Workshop Electron. Grid EGRID*, 2023, pp. 1–6.

[23] P. Tenti and T. Caldognetto, "Integration of local and central control empowers cooperation among prosumers and distributors towards safe, efficient, and cost-effective operation of microgrids," *Energies*, vol. 16, no. 5, Jan. 2023, Art. no. 2320.

[24] P. Tenti and T. Caldognetto, "Generalized control of the power flow in local area energy networks," *Energies*, vol. 15, no. 4, Jan. 2022, Art. no. 1416.

[25] K. S. Yildirim, R. Carli, L. Schenato, and M. Todescato, "A distributed dual-ascent approach for power control of wireless power transfer networks," in *Proc. IEEE 56th Annu. Conf. Decis. Control*, 2017, pp. 3507–3512.

[26] S. Boyd, N. Parikh, E. Chu, B. Peleato, and J. Eckstein, "Distributed optimization and statistical learning via the alternating direction method of multipliers," *MAL*, vol. 3, no. 1, pp. 1–122, Jul. 2011.

[27] J. A. Nelder and R. Mead, "A simplex method for function minimization," *Comput. J.*, vol. 7, no. 4, pp. 308–313, Jan. 1965.

[28] S. A. Alghunaim and A. H. Sayed, "Linear convergence of primal–dual gradient methods and their performance in distributed optimization," *Automatica*, vol. 117, Jul. 2020, Art. no. 109003.
[29] T. Caldognetto, A. Petucco, A. Lauri, and P. Mattavelli, "A flexible power electronic converter system with rapid control prototyping for research and teaching," *HardwareX*, vol. 14, Jun. 2023, Art. no. e00411.
[30] K. Strunz, "Benchmark Systems for network integration of renewable and distributed energy resources," CIGRE, Paris, France, Tech. Rep. C6.04.02, 2009.
[31] "Solar power generation data," Aug. 2020. Accessed: Dec. 3, 2023. [Online]. Available: https://www.kaggle.com/datasets/anikannal/solar-power-generation-data?select=Plant_1_Generation_Data.csv
[32] "Wind turbine scada dataset," Mar. 2019. Accessed: Dec. 3, 2024. [Online]. Available: https://www.kaggle.com/datasets/berkerisen/wind-turbine-scada-dataset
[33] D. A. Broden, K. Paridari, and L. Nordstrom, "Matlab applications to generate synthetic electricity load profiles of office buildings and detached houses," in *Proc. IEEE Innov. Smart Grid Technol. - Asia ISGT-Asia*, Dec. 2017, pp. 1–6.
[34] Fronius, "(No Date) Technical details - fronius symo 17.5," Feb. 2017. Accessed: May 12, 2023. [Online]. Available: https://web.archive.org/web/20220701145818/https://www.fronius.com/it-it/italy/energia-solare/installatori-e-partner/dati-tecnici/tutti-i-prodotti/inverter/fronius-symo/fronius-symo-17-5-3-m
[35] Aurora, "PVI-12.5-OUTD inverter datasheet," Mar. 2010. Accessed: May 12, 2023. [Online]. Available: http://www.test-italy.com/Energia_Alternativa/Test%20Energia/PDF_inverter/power-one/PVI-10.0-12.5/pvi100125it.pdf
[36] Imperix, "B-Board PRO Embeddable Controller," Accessed: Jun. 7, 2024. [Online]. Available: https://imperix.com/wp-content/uploads/document/B-Board_Datasheet.pdf
[37] A. Lauri, T. Caldognetto, D. Biadene, and P. Mattavelli, "An unbalance and power controller allowing smooth islanded transitions in three-phase microgrids," *IEEE Trans. Ind. Electron.*, early access, Jan. 19, 2024, doi: 10.1109/TIE.2023.3347836.
[38] *IEEE Standard for the Specification of Microgrid Controllers*, IEEE Standard 2030.7-2017, Apr. 2018.

ANDREA LAURI (Graduate Student Member, IEEE) received the B.Sc. and M.S. degrees in electronics engineering from the University of Padova, Padova, Italy, in 2018 and 2022, respectively. He is currently working toward the Ph.D. degree in mechatronics engineering with the University of Padova, Vicenza, Italy. His research interests include modeling and control of grid-connected inverters in microgrids.

TOMMASO CALDOGNETTO (Senior Member, IEEE) received the M.S. degree (Hons.) in electronics engineering and the Ph.D. degree in information engineering from the University of Padova, Padova, Italy, in 2012 and 2016, respectively. He is currently an Assistant Professor with the Department of Management and Engineering, University of Padova, Vicenza, Italy. His research interests include the control of grid-tied converters, microgrid architectures, converters for DC nanogrids, and real-time simulation for power electronics applications. Since 2019, he has been an Associate Editor for IEEE OPEN JOURNAL OF POWER ELECTRONICS.

RUGGERO CARLI (Member, IEEE) received the Laurea degree in computer engineering and the Ph.D. degree in information engineering from the University of Padova, Padua, Italy, in 2004 and 2007, respectively. From 2008 to 2010, he was a Postdoctoral Fellow with the Department of Mechanical Engineering, University of California at Santa Barbara, Santa Barbara, CA, USA. He is currently an Associate Professor with the Department of Information Engineering, University of Padova. His research interests include distributed algorithms for optimization, estimation, and control over networks, nonparametric estimation, and learning for robotics.

DAVIDE BIADENE (Member, IEEE) received the M.S. degree in electronic engineering and the Ph.D. degree in information engineering from the University of Padova, Padova, Italy, in 2014 and 2017, respectively. He is currently a Research Fellow with the Department of Management and Engineering, University of Padova, Vicenza, Italy. In 2016, he was a visiting Ph.D. student with the Power Electronic Systems Laboratory, Department of Information Technology and Electrical Engineering, ETH Zurich, Zurich, Switzerland. From 2017 to 2021, he was an R&D Test Engineer in the automotive business line team with Infineon Technologies Italia. His research interests include DC-DC converters for renewables and energy storage devices.

PAOLO MATTAVELLI (Fellow, IEEE) received the M.S. degree (Hons.) and the Ph.D. degree in electrical engineering from the University of Padova, Padua, Italy, in 1992 and 1995, respectively. From 1995 to 2001, he was a Researcher with the University of Padova. From 2001 to 2005, he was an Associate Professor with the University of Udine, Udine, Italy, where he led the Power Electronics Laboratory. In 2005, he joined the University of Padova, Vicenza, Italy, with the same duties. From 2010 to 2012, he was with the Center for Power Electronics Systems, Virginia Tech. He is currently a Professor with the University of Padova. He is leading several industrial and Government projects in his research areas which include analysis, modeling, analog, and digital control of power converters, grid-connected converters for renewable energy systems and micro-grids, high-temperature, and high-power density power electronics. His google scholar H-index is 81. From 2003 to 2012, he was an Associate Editor for IEEE TRANSACTIONS ON POWER ELECTRONICS. From 2005 to 2010, he was the Industrial Power Converter Committee Technical Review Chair for the IEEE TRANSACTIONS ON INDUSTRY APPLICATIONS. During 2003–2006, 2006–2009, and 2013–2015, he was a member-at-large of the IEEE Power Electronics Society's Administrative Committee. He was the recipient of the Prize Paper Award in the IEEE TRANSACTIONS ON POWER ELECTRONICS in 2005, 2006, 2011, and 2012, and 2nd Prize Paper Award at the IEEE Industry Application Annual Meeting in 2007. He is the Co-Editor in Chief of IEEE TRANSACTIONS ON POWER ELECTRONICS.

Open Access funding provided by 'Università degli Studi di Padova' within the CRUI CARE Agreement